Precision Engineering 38 (2014) 221–229

Contents lists available at ScienceDirect

Precision Engineering

journal homepage: www.elsevier.com/locate/precision

Technical note

Development of a micro-drilling burr-control chart for PCB drilling

Binayak Bhandari[a], Young-Sun Hong[a], Hae-Sung Yoon[a], Jong-Seol Moon[a], Minh-Quan Pham[a], Gyu-Bong Lee[b], Yuchu Huang[c], Barbara S. Linke[c], D.A. Dornfeld[c], Sung-Hoon Ahn[a,*]

[a] School of Mechanical & Aerospace Engineering, Seoul National University, Seoul 151-742, Republic of Korea
[b] Korea Institute of Industrial Technology (KITECH), Cheonan-si 330-825, Republic of Korea
[c] Laboratory for Manufacturing and Sustainability, University of California, Berkeley, CA 94720-1740, United States

ARTICLE INFO

Article history:
Received 17 April 2012
Received in revised form 11 July 2013
Accepted 29 July 2013
Available online 7 August 2013

Keywords:
Micro drilling
PCB
Drilling burr control
Taguchi method
Burr classification
S/N ratio

ABSTRACT

A drilling burr-control chart (DBCC), based on experimental results, is a tool for the prediction and control of drilling burrs for a large range of drilling parameters. A micro-drilling burr-control chart (M-DBCC) was developed for a standard double-sided copper-clad laminated (CCL) printed circuit board (PCB) with laminated fiber-reinforced plastic (FRP) substrate. This chart will assist in the selection of favorable drilling parameters for predicting and achieving preferred types of burrs. Burr classification was carried out according to the burr geometric characteristics, burr formation mechanisms, burr height, and drill bit breakage while drilling. The design of experiment (DOE) technique based on the Taguchi method was used to find the most significant drilling parameter affecting burr height. The results show that the drill diameter makes a statistically significant contribution to burr-height variation.

1. Introduction

A printed circuit board (PCB) is a thin plate made of one or more layers of insulating board (also known as substrate), which supports electronic components and connects them electrically, using conductive pathways, tracks, or signal traces [1]. PCBs are found in almost every kind of electronic device, ranging from toys to sophisticated radar systems.

There are three major types of PCB construction: single-sided, double-sided, and multi-layered. In single-sided construction, all components are placed on one side of the board. Double-sided PCBs are used when the number of components is too large to allow single-sided construction within the designated space. A multi-layered board has several printed circuit layers separated by layers of insulation. The electronic components on the surface are connected through plated holes drilled down to the appropriate circuit layer, which simplifies the circuit.

The most common substrate used for PCBs is made of glass-fiber-reinforced epoxy resin with copper foil bonded to the surface (single- or double-sided).

Drilling provides the holes for the electronic components to be placed on PCB surfaces. Burrs are thereby created on both the entrance and exit surfaces of a PCB [2]. In engineering, a burr refers to a raised edge on a metal part, and appears in many contexts, including filed wires, raised portions of a surface, etc. In the PCB manufacturing industry, most of the operations are automatically controlled by computer programs, except for the drilling operation, which is usually the bottleneck station [3]. Micro-drilling in PCBs presents greater problems, since coolant-fed drills cannot be used. In general, high spindle speed and high infeed are recommended for PCB drilling operations. However, this might not be always cost-effective, because a large amount of time must be devoted to deburring operations after drilling. A multitude of ideas [4–7] have been proposed by researchers and engineers to achieve burrless drilling, but thus far, these efforts have met with only partial success.

In the drilling process, burrs are produced on both the entrance and exit surfaces of the workpiece. However, the formation mechanisms are different. Entrance burrs are formed via plastic flow, while exit burrs are formed as the material extends off the exit surface of the workpiece [8]. Generally, exit burrs are larger than entrance burrs, and are undesirable because they cause most burr-related problems, such as interference with the assembly of parts, which leads to jamming and misalignment, reduces the fatigue life of the parts, and acts as a crack initiation point and safety hazard. Deburring is often required, but in the case of micro-drilling, manual removal of burrs is not practical, and sometimes even impossible.

* Corresponding author. Tel.: +82 2 880 7110; fax: +82 2 883 0179.
E-mail address: ahnsh@snu.ac.kr (S.-H. Ahn).

0141-6359/$ – see front matter © 2013 Elsevier Inc. All rights reserved.
http://dx.doi.org/10.1016/j.precisioneng.2013.07.010

Table 1
Parameters affecting burr formation while drilling.

Category	Parameters
Drill geometry	Point geometry, point angle, helix angle, relief angle
Drill bit material	Hardness, strain-hardening characteristics, ductility, toughness, thermal properties
Cutting conditions	Cutting speed, spindle speed, infeed, lubrication, use of coolant, retract rate, chip load
Others	Tool wear, machined material, built-up-edge, entry materials, exit materials, dwell time between drill hits, drill bit clogging, temperature

Several earlier burr-related studies [6,9] have been based on experiments rather than analytical methods, due to the complex burr-formation mechanism, which is further influenced by a number of parameters, including drill geometry, workpiece material, drilling conditions and environmental factors. Watanabe et al. [10] studied the influence of the radial run-out of micro-drills on the hole quality. Hinds and Treanor [11] used finite element methods to analyze the stresses occurring in micro-drills. They used three-dimensional models of the drills, and performed experimental tests to determine the drill loading. Furthermore, many published studies of drilling burrs [6,8] have been concerned with isotopic and tensile materials, such as various steels.

Our study focuses on the development of a micro-drilling burr-control chart (M-DBCC) for PCB board substrates, which are made of composite material and are brittle in nature. A drilling burr-control chart (DBCC) is a tool developed on the basis of experimental results for predicting and controlling drilling burrs under a wide range of drilling conditions [12]. This chart also assists in selecting the cutting parameters to obtain a preferred type of burr.

2. Burr formation mechanisms

There is no generally accepted analytical model for controlling and predicting the mechanisms of burr formation. This is mainly because the drilling mechanism itself is a complicated phenomenon, affected by many parameters, which are listed in Table 1. It is even more complicated in the case of layered composite drilling (e.g., PCB drilling), since additional phenomena such as delamination are caused by heat built-up while drilling. However, the present paper focuses on burr formation, without taking heat generation during the drilling process into account.

The thrust force of the drilling process is affected by the ratio of the feed (infeed (mm/s)/spindle speed (rev/s)) to the drill diameter (μm). The plastic deformation of the exit surface, which influences the burr formation, is determined by the thrust force. Increased feed while drilling increases the thrust force. A correlation between the feed and the thrust force with varying drill diameters can be approximated using the orthogonal cutting model described in [8]. The cutting edge of the drill is assumed to be divided into many segments, and an orthogonal cutting model is applied to each segment, as shown in Fig. 1. Where, *Res* is the resultant force, *F* is friction force, *N* is normal force to friction, F_s is shear force, F_n is normal force to shear and F_c is the cutting force. The thrust force exerted on each segment is represented as

$$\Delta F_t = \frac{kf \sin\kappa \sin(\lambda-\alpha)}{2\sin\varphi\cos(\varphi+\lambda-\alpha)}\Delta W \tag{1}$$

$$\Delta W = \frac{(\rho_{i+1}-\rho_i)R}{\sin\kappa} \quad \text{for } i = 1, 2, \ldots, n \tag{2}$$

ρ is the relative radius r/R, which is the ratio of the distance, from the drill center to the segment, to the drill radius.

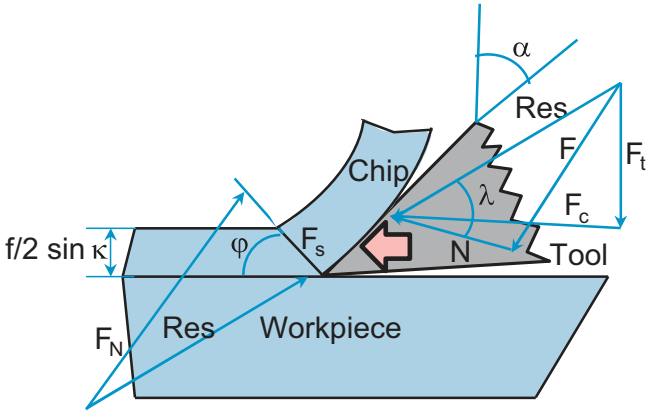

Fig. 1. Orthogonal cutting model.

For the chisel edge of a split point twist drill, a constant rake angle can be assumed and therefore the total thrust force F_t is given by

$$F_t = \sum_{i=1}^{n}(\Delta F_{t,\text{chisel edge}} + \Delta F_{t,\text{cutting edge}}) \tag{3}$$

$$F_t = \sum_{i=1}^{n}(k \cdot f \cdot R \cdot f_n(\varphi \cdot \lambda \cdot \delta \cdot h \cdot \kappa)) \tag{4}$$

where k is the shear strength of the workpiece material, f_n is a function of (φ, λ, δ, h, κ), f is the feed (mm/rev), 2κ is the point angle of the drill, λ is the friction angle, α is the tool rake angle, φ is the shear plane angle, R is drill radius, δ is the ratio of the web thickness to the drill diameter, and h is the helix angle. The burr formation mechanism is influenced by stress and resultant strain. The effective stress can be represented as follows:

$$\tilde{\sigma} = \frac{F_t}{A} \propto \frac{F_t}{d^2} \tag{5}$$

where F_t is the thrust force, which is a function of the feed rate (f), diameter (d), drill bit, and workpiece material.

$$\tilde{\sigma} = \frac{f}{d} f_n(\text{Material}(k, \lambda),\ \text{Geometry}(\varphi, \delta, h, \kappa)) \tag{6}$$

For a given drill geometry and workpiece material, burr formation is determined solely by f/d, which is the dimensionless feed parameter (F_n) in the M-DBCC. The cutting speed parameter (S) is defined as the product of the drill diameter (μm) and spindle speed (N), and its units are μm/min.

$$F_n = \frac{f}{d} \tag{7}$$

$$S = K \times d \times N \tag{8}$$

where N = spindle speed (min^{-1}), d = drill bit diameter (μm), f = feed (mm/rev), and K is a constant that makes the orders of the two equations equal. N, d, and f are the parameters of the M-DBCC.

3. Classification of burr types

There are three types of burrs, depending on location: (a) entrance burrs, (b) interlayer burrs, and (c) exit burrs. An entrance burr is created on the side of the workpiece where the drill enters. This type of burr is usually very small, and may be removed without much difficulty by chamfering the hole. Interlayer burrs occur at the junction of two layers of a PCB, and depend on the combination of materials in the upper and the lower layers, as well as the

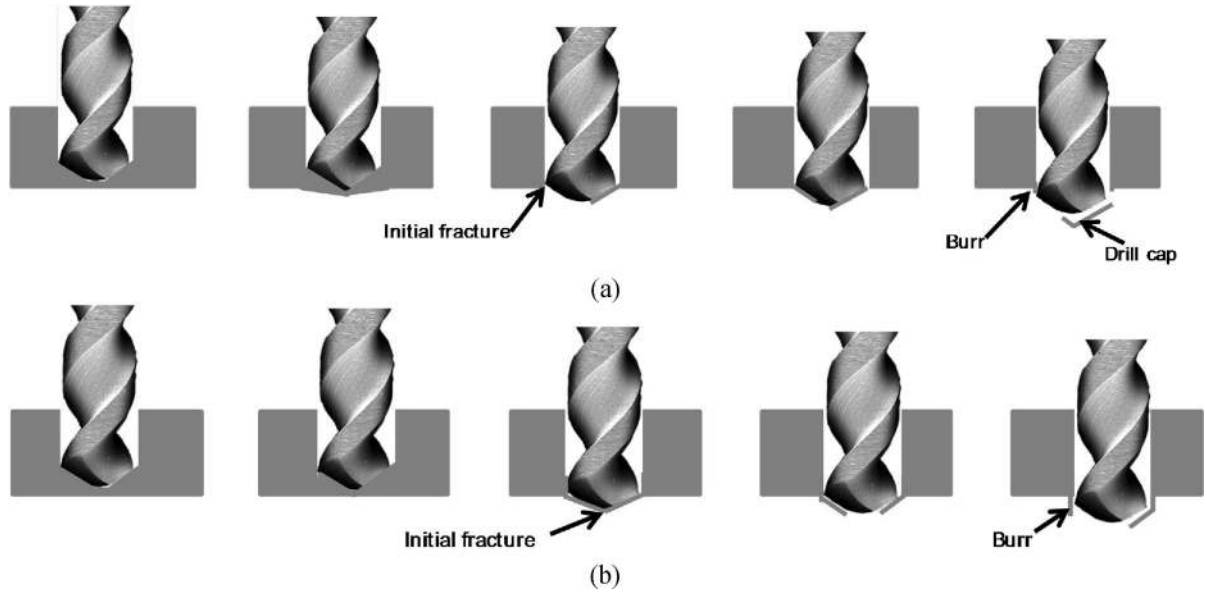

Fig. 2. Classification of burr types: (a) uniform burr and (b) transient burr (redrawn from [8]).

thickness of the sealant between the layers (if any) and the process parameters. In the presence of a thick sealant, exit burrs are fully developed from the upper layer. Exit burrs are larger than entrance burrs, and hence the exit burrs of a PCB stack are mainly considered for study [13].

Depending on their nature, and based on size, we have classified PCB burrs into (a) uniform burrs and (b) transient burrs. Uniform burrs have relatively small and unvarying heights around the periphery of a drilled hole. As the drill approaches the exit surface, the material under the chisel edge begins to deform. The distance from the exit surface to the point where the deformation begins depends mainly on the thrust force while drilling. As the drill advances, the plastic deformation zone expands from the center to the edge of the drill. Finally, an initial fracture occurs at the end of the cutting edge. When the drill exits, a small portion of the material is bent and pushed out ahead to create a uniform burr, as shown in Fig. 2(a).

In a transient burr, a higher thrust force, due to higher infeed, causes a large portion of the drill exit surface to be pushed out, resulting in a large material flow from the exit surface. In PCB drilling, transient burrs are larger, irregular, and non-uniformly distributed. The formation mechanism of a transient burr is shown in Fig. 2(b).

Table 2
Specifications of the drill bits.

Helix angle	35°
Point angle	130°
1st relief angle	15°
2nd relief angle	30°

4. Experiments

4.1. Micro-drill bit

Due to the trend toward highly efficient, low-cost, and downsized electric parts, there is an increasing demand for micro-machining [14], and for drills that are smaller in diameter and capable of drilling a wider variety of materials. The diameter of the smallest drill in use today is only about 50 μm, which is about the thickness of a human hair. In our experiments, split-point twist drills with tungsten carbide (WC) tips and high-speed steel

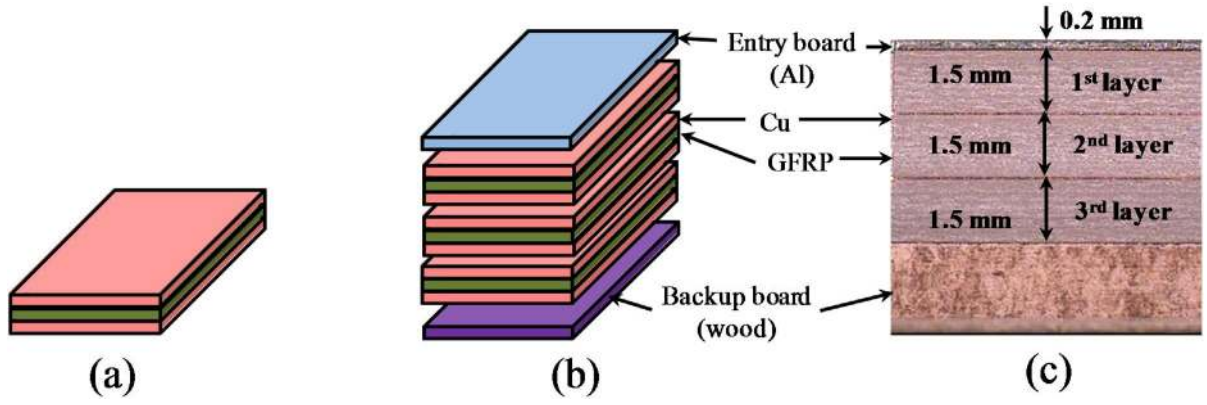

Fig. 3. (a) Copper-clad laminated double-sided PCB with GFRP substrate, (b) PCB stacking for drilling, and (c) cross-section of the PCB stack.

Table 3
Experimental parameters and their levels.

Factors	Level 1	Level 2	Level 3
Infeed (mm/s)	30	40	50
Spindle speed (min^{-1})	90,000	60,000	30,000
Drill diameter (μm)	400	600	800

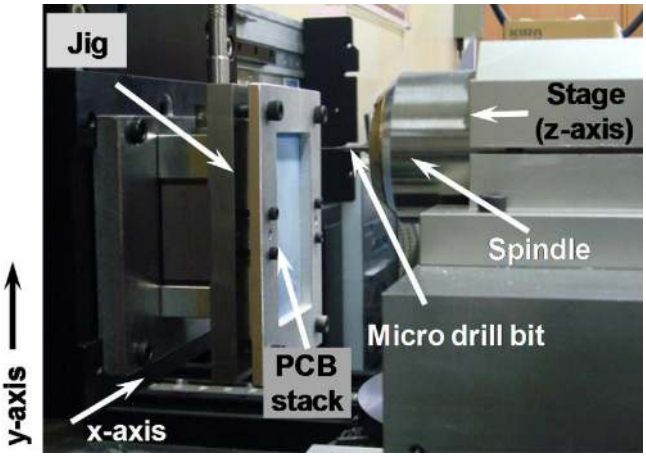

Fig. 4. Drilling experimental setup.

(HSS) shanks were used, having diameters of 400 μm, 600 μm, and 800 μm. The micro-drill bits used in the experiments were manufactured by Neo Technical System Co., Ltd., Korea, and their specifications are listed in Table 2.

4.2. Experimental setup

Three stacks of double-sided copper-clad laminated (CCL) PCBs were used in the experiments. The lower part of a stack was supported by a wooden backup board, and an aluminum entry board was placed on the top of the stack for heat dissipation (a standard procedure in PCB drilling). These were clamped together, as shown in Fig. 3(b). Fig. 3(c) shows a cross-section of the PCB stack.

A three-axis stage (Justek Inc., Korea) and a high-speed spindle (D1733, Westwind Air Bearings, United Kingdom) were used in the drilling experiments. The experimental setup is shown in Fig. 4. Three drilling trials were conducted for each set of designed experiments. The experiments were performed at standard room temperature (22 °C), and natural convection was allowed, without application of any external cooling to the workpiece. In Cases I and III, the experiments were conducted by varying the drilling parameters until bit breakage occurred. New drill bits were used in every set of experiments. A field-emission scanning electron microscope (FESEM) was used to measure the burr height.

5. Design of experiment

5.1. Fractional factorial design

A fractional matrix of experiments was used instead of a full matrix to reduce the number of experiments. The design of experiment (DOE) technique was performed, in which the following three cases were considered for each drill bit size (400 μm, 600 μm, and 800 μm).

Case I: Varying spindle speed (min^{-1}), constant infeed (mm/s).
Case II: Varying infeed (mm/s), constant spindle speed (min^{-1}).
Case III: Varying infeed (mm/s) and spindle speed (min^{-1}).

From the above DOE, the significance of the experimental parameters and their relevance to the experiment were easily understood. The current standard drilling conditions in the PCB industry for a 400-μm drill are a spindle speed (N) of 90,000 min^{-1} and an infeed of 40 mm/s. The designed experimental conditions included the standard conditions.

5.2. Taguchi design

The effects of many different parameters on performance characteristics can be concisely examined using the orthogonal array experimental design proposed by Genichi Taguchi. This DOE can be used to estimate the main effects using only a few experimental cases. The infeed (mm/s), spindle speed (min^{-1}), and drill diameter (μm) were chosen as controllable parameters affecting the burr size. Altogether, three levels were selected for each parameter, and an L9 (3^3) orthogonal array (OA) of experiments was performed. L9 means that the array required 9 runs, and 3^3 indicates that the design estimated up to three main effects at 3 levels each. Table 3 lists the experimental parameters (viz., infeed, spindle speed, and drill diameter) and their levels.

A spindle speed of 90,000 min^{-1} and an infeed of 40 mm/s are standard practice for a 400-μm drill diameter in the PCB industry. As the diameter of the drill bit increases, the spindle speed and feed rate decrease. All parameters were varied in two directions from the standard machining conditions, except for the 400-μm drill diameter. The parameter levels were selected for ease of comparison, and to find a correlation between the parameters and the burr size.

Table 4
Drill bit conditions for Case I (varying spindle speed of 90,000–5000 min^{-1} and constant infeed of 30 mm/s), and the corresponding S and F_n values.

Drill diameter (μm)	Spindle speed (min^{-1})	Infeed (mm/s)	Drill bit condition		Burr chart functions					
			OK	$Broken_{(dia)}$	$S_{(400)}$	$F_{n(400)}$	$S_{(600)}$	$F_{n(600)}$	$S_{(800)}$	$F_{n(800)}$
400, 600, 800	90,000	30	$\surd_{(all)}$		0.36	0.050	0.54	0.033	0.72	0.025
400, 600, 800	80,000	30	$\surd_{(all)}$		0.32	0.056	0.48	0.037	0.64	0.028
400, 600, 800	70,000	30	$\surd_{(all)}$		0.28	0.064	0.42	0.042	0.56	0.032
400, 600, 800	60,000	30	$\surd_{(all)}$		0.24	0.075	0.36	0.050	0.48	0.037
400, 600, 800	50,000	30	$\surd_{(all)}$		0.20	0.090	0.30	0.060	0.40	0.045
400, 600, 800	40,000	30	$\surd_{(all)}$		0.16	0.112	0.24	0.075	0.32	0.056
400, 600, 800	30,000	30	$\surd_{(all)}$		0.12	0.150	0.18	0.100	0.24	0.075
400, 600, 800	20,000	30	$\surd_{(all)}$		0.08	0.225	0.12	0.150	0.16	0.112
400, 600, 800	10,000	30	$\surd_{(800)}$	$\surd_{(400,\,600)}$	0.04	0.450	0.06	0.300	0.08	0.225
800	9000	30	$\surd_{(800)}$		–	–	–	–	0.072	0.25
800	5000	30		$\surd_{(800)}$	–	–	–	–	0.04	0.45

Table 5
Drill bit conditions for Case II (constant spindle speed of 90,000 min^{-1} and varying infeed of 30–90 mm/s), and the corresponding S and F_n values.

Drill diameter (μm)	Spindle speed (min^{-1})	Infeed (mm/s)	Drill bit condition		Burr chart functions					
			OK	Broken$_{(dia)}$	$S_{(400)}$	$F_{n(400)}$	$S_{(600)}$	$F_{n(600)}$	$S_{(800)}$	$F_{n(800)}$
400, 600, 800	90,000	30	√$_{(all)}$		0.36	0.050	0.54	0.033	0.72	0.025
400, 600, 800	90,000	40	√$_{(all)}$		0.36	0.066	0.54	0.044	0.72	0.033
400, 600, 800	90,000	50	√$_{(all)}$		0.36	0.083	0.54	0.055	0.72	0.041
400, 600, 800	90,000	60	√$_{(all)}$		0.36	0.100	0.54	0.066	0.72	0.050
400, 600, 800	90,000	70	√$_{(all)}$		0.36	0.116	0.54	0.077	0.72	0.058
400, 600, 800	90,000	80	√$_{(all)}$		0.36	0.133	0.54	0.088	0.72	0.067
400, 600, 800	90,000	90	√$_{(all)}$		0.36	0.150	0.54	0.100	0.72	0.075

Table 6
Drill bit conditions for Case III (varying spindle speed of 90,000–9000 min^{-1} and varying infeed of 30–120 mm/s), and the corresponding S and F_n values.

Drill diameter (μm)	Spindle speed (min^{-1})	Infeed (mm/s)	Drill bit condition		Burr chart functions					
			OK	Broken$_{(dia)}$	$S_{(400)}$	$F_{n(400)}$	$S_{(600)}$	$F_{n(600)}$	$S_{(800)}$	$F_{n(800)}$
400, 600, 800	90,000	30	√$_{(all)}$		0.36	0.050	0.54	0.033	0.72	0.025
400, 600, 800	80,000	40	√$_{(all)}$		0.32	0.075	0.48	0.050	0.64	0.037
400, 600, 800	70,000	50	√$_{(all)}$		0.28	0.107	0.42	0.071	0.56	0.053
400, 600, 800	60,000	60	√$_{(all)}$		0.24	0.150	0.36	0.100	0.48	0.075
400, 600, 800	50,000	70	√$_{(all)}$		0.20	0.210	0.30	0.140	0.40	0.105
400, 600, 800	40,000	80	√$_{(all)}$		0.16	0.300	0.24	0.200	0.32	0.150
400, 600, 800	30,000	90	√$_{(all)}$		0.12	0.450	0.18	0.300	0.24	0.225
400, 600, 800	20,000	100	√$_{(all)}$		0.08	0.750	0.12	0.500	0.16	0.375
400, 600, 800	10,000	110	√$_{(800)}$	√$_{(400, 600)}$	0.04	1.650	0.06	1.100	0.08	0.825
800	9000	120		√$_{(800)}$	–	–	–	–	0.072	1.0

6. Results and discussion

6.1. Drill bit condition

There are two different types of drill-bit breakage: deflected breakage and twisted breakage. The former is caused by radial force, and the breakage is at the end of flute, whereas the latter is caused by high torque, and the breakage is normally in the middle of the flute.

In our experiments, all drilling parameters were gradually varied. The spindle speed was initially set at 90,000 min^{-1}, and was gradually reduced to 10,000 min^{-1} in 10,000 min^{-1} steps. The infeed was gradually increased from 30 mm/s in steps of 10 mm/s until the drill bit broke. The main reason for performing drilling experiments that continue until bit breakage occurs is to determine the various combinations of parameters leading to breakage. The smaller drill bits (with diameters of 400 μm and 600 μm) broke at 10,000 min^{-1} for an infeed of 30 mm/s (Case I) and an infeed of 110 mm/s (Case III), verifying that the lower spindle speed plays a greater role in micro-drill-bit breakage than infeed. For the 800-μm drills, the spindle speed was further reduced, as shown in Tables 4 and 6, until the bits broke. No drill bits were reported broken in the experiment with a constant spindle speed of 90,000 min^{-1} and varying infeed (30–90 mm/s), as Table 5 indicates. The experimental results obtained under the drill bit conditions of Cases I–III with 400-μm, 600-μm, and 800-μm drills, and the corresponding burr chart functions calculated via Eqs. (7) and (8) are listed in Tables 4–6.

6.2. Drilling burr shape

In PCB drilling, the burr shape is important, since the quality of the hole and the burr size can be approximated from it. Thus, before taking an FESEM image of a burr, each drilled PCB was carefully placed in a sonicator (Mujigae Analog SD-80H, Korea) with an ultrasonic frequency of 40 kHz for 5–10 s to remove the debris produced during PCB drilling. All the burrs considered in this study are from the exit surfaces of the third layer.

Fig. 5 shows the FESEM images from the 400-μm drilling experiments with a constant infeed of 30 mm/s and varying spindle speed (Case I). As the figures indicate, all workpieces had small, uniform burrs around the periphery of the drilled hole. Hence, all of the burrs fell into the uniform category. Fig. 6 shows the FESEM images from the 400-μm drilling experiments with a constant spindle speed of 90,000 min^{-1} and varying infeed (Case II). All workpieces but one (Fig. 6(a)) had large, irregular, non-uniformly distributed burrs, which placed them in the transient burr category. Fig. 7 shows the

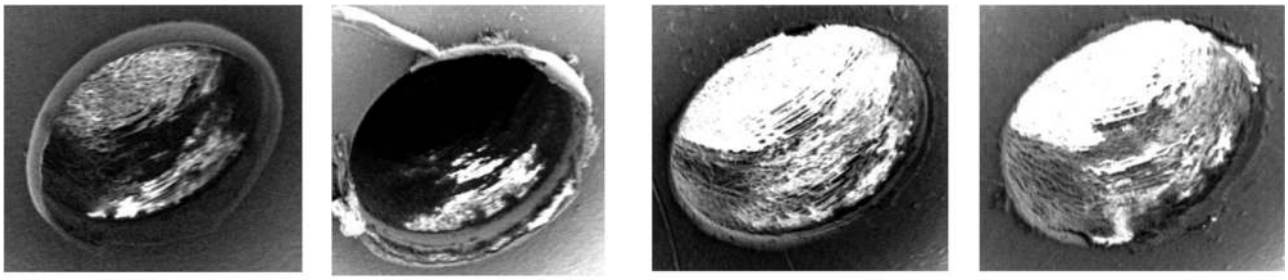

Fig. 5. FESEM images from the 400-μm drilling experiments with a constant infeed of 30 mm/s and varying spindle speed.

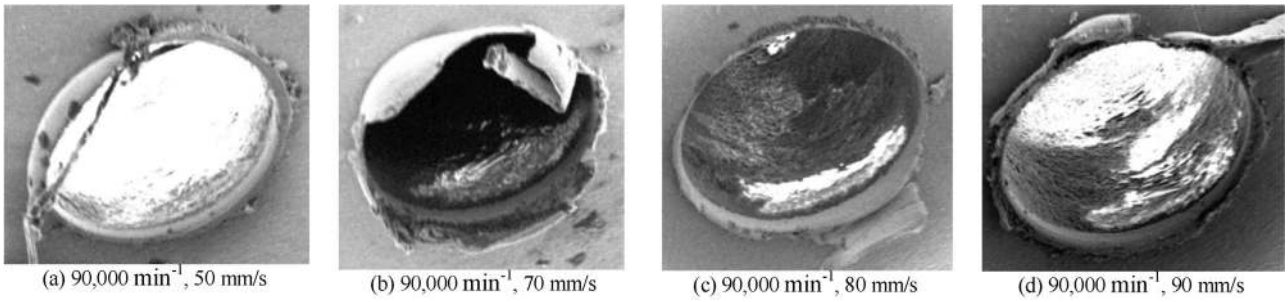

Fig. 6. FESEM images from the 400-μm drilling experiments with a constant spindle speed of 90,000 min^{-1} and varying infeed.

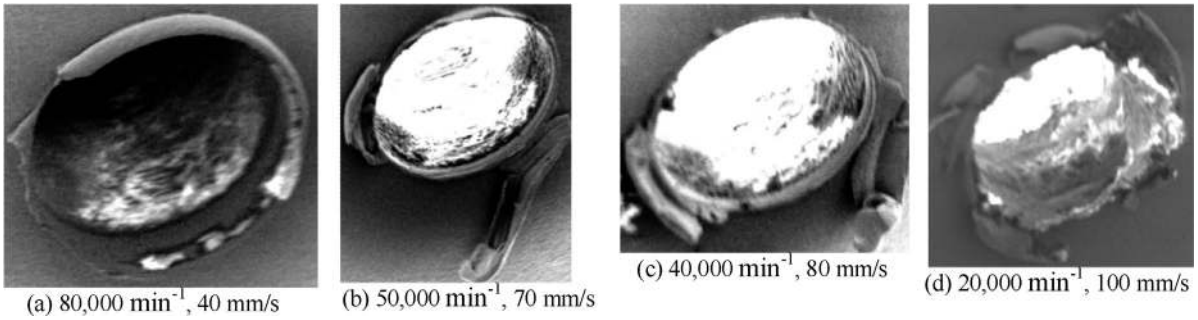

Fig. 7. FESEM images from the 400-μm drilling experiments with varying infeed spindle speed.

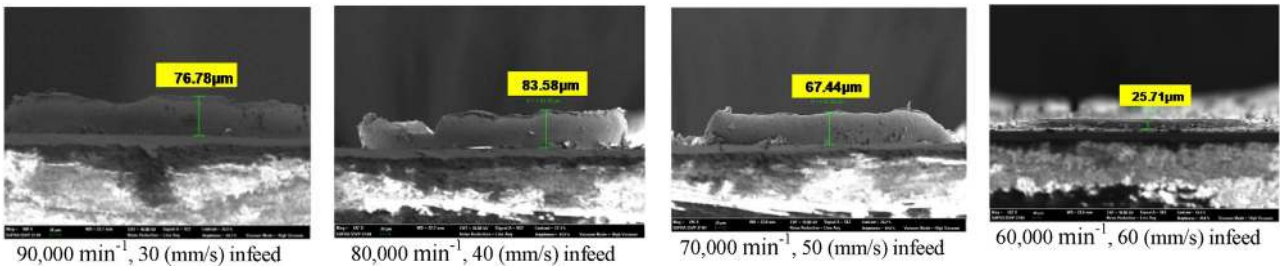

Fig. 8. Burr height measured by FESEM (600-μm drill bit, Case III).

FESEM images from the 400-μm drilling experiments with varying infeed and spindle speed (Case III). As in the previous case, all burrs except those of Fig. 7(a) fell into the transient burr category. All of these images (Figs. 5–7) were exit burrs taken with the workpiece inclined at 45° relative to the horizontal plane.

6.3. Drilling burr height

Prior to taking the FESEM images, fine grinding was applied to each PCB edge, as close as 500 μm from the burr surface, for clear imaging. The workpiece was then subjected to 5–10 s of sonication to remove the debris produced during grinding, following which sputtering was performed. Each workpiece was placed vertically in the FESEM chamber, and an FESEM image was taken. Figs. 8 and 9 show the drilling burr heights (Case III) for the 600-μm and 800-μm drilling experiments, respectively. It can be inferred from these figures that under the same machining conditions, the burr heights were greater for a smaller drilling diameter.

6.4. Taguchi experimental results

Taguchi experiments were performed to determine the relationship between the drilling parameters and the burr height. The three independent variables in the Taguchi experiments were spindle speed (min^{-1}), infeed (mm/s), and drill diameter (μm); the dependent variable was burr height (μm). Three drilling trials were

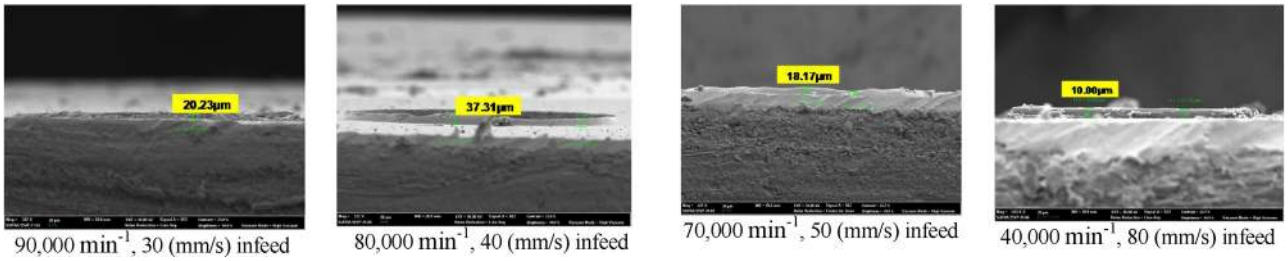

Fig. 9. Burr height measured by FESEM (800-μm drill bit, Case III).

Table 7
L9 (3^3) Taguchi orthogonal array.

S. no.	Infeed (mm/s)	Spindle speed (min^{-1})	Drill dia (μm)	S	F_n	Drill bit condition
1	1 (30)	1 (90,000)	1 (400)	0.36	0.05	√
2	1 (30)	2 (60,000)	2 (600)	0.36	0.05	√
3	1 (30)	3 (30,000)	3 (800)	0.24	0.075	√
4	2 (40)	1 (90,000)	2 (600)	0.54	0.04	√
5	2 (40)	2 (60,000)	3 (800)	0.48	0.05	√
6	2 (40)	3 (30,000)	1 (400)	0.12	0.2	√
7	3 (50)	1 (90,000)	3 (800)	0.72	0.04	√
8	3 (50)	2 (60,000)	1 (400)	0.24	0.125	√
9	3 (50)	3 (30,000)	2 (600)	0.18	0.16	√

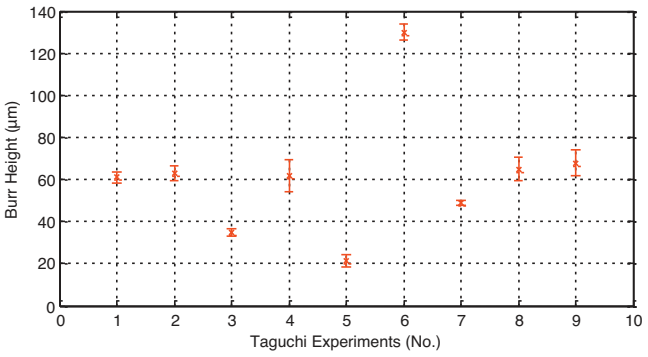

Fig. 10. Average burr heights from the Taguchi experiments, plotted with error bars.

conducted for each set of experiments. New drill bits were used for every set of experiments. Table 7 shows the L9 (3^3) Taguchi orthogonal array, containing the infeed, spindle speed, drill diameter, burr chart functions, and drill bit condition. No drill-bit breakage was reported for any of the experiments. The reported burr height was the average of the maximum burr heights for the three trials. The corresponding error bars are shown in Fig. 10.

Multiple regression tests were performed to analyze the results of the OA experiments, and to determine the burr-height variation contributed by each parameter. Statistical Product and Service Solutions (SPSS 19) was used for the analysis. A p-value of 0.05 was chosen as the significance level.

Table 8 summarizes the results of the regression tests. The probability values (p-values) for the drill diameter were less than 0.05, indicating that the drill diameter made a statistically significant contribution to the burr-height variation. Contrary to general intuition, the smaller drill bits produced larger burrs.

Standardized multiple regression coefficients (beta coefficients) are estimates resulting from an analysis of variables that have been standardized so that their variances are 1. In a multiple regression analysis, standardization is usually carried out to answer the question of which independent variable has a greater effect on the dependent variable, when the variables are measured in different units. Comparison of the standardized coefficient (beta) values indicated that the drill diameter (beta = −0.726) had the greatest effect on the burr height, followed by the spindle speed (beta = −0.296) and infeed (beta = 0.110).

Table 8
Standardized beta values and p-values, indicating the statistically significant parameter.

Model	Parameters	Beta	p value
1	Drill diameter (μm)	−0.726	0.027*
2	Drill diameter (μm)	−0.726	0.029*
	Spindle speed (min^{-1})	−0.296	0.287
3	Drill diameter (μm)	−0.726	0.045*
	Spindle speed (min^{-1})	−0.296	0.328
	Infeed (mm/s)	0.110	0.703

6.5. Correlation between burr height, spindle speed, drill diameter, and feed rate

Using the results of the multi-variable regression analysis, a correlation between the burr height, spindle speed (N, min^{-1}), drill diameter (d, μm), and infeed rate (f, mm/s) was obtained for PCB drilling. The equation can be expressed as follows:

$$\text{Burr height} = 142.619 + 0.00034 \times N - 0.126 \times d + 0.384 \times f, \quad R^2 = 0.626 \tag{9}$$

In the above equation, the slope with respect to the spindle speed is 0.00034.

6.6. Analysis of the S/N ratio

To determine the effect of each variable on the output, experimental results are transformed into a signal-to-noise (S/N) ratio. In the Taguchi method, the term 'signal' and 'noise' represents the desirable value and undesirable value for the output characteristics. Taguchi recommends the use of the S/N ratio to measure the quality characteristics deviating from the desired values. There are three cases of S/N ratios, nominal the better characteristics, smaller the better characteristics and bigger the better characteristics. Eqs. (10)–(12) are used for above cases respectively.

$$\text{SN}_i = 10 \log \frac{\bar{y}_i^2}{s_{y_i}^2} \tag{10}$$

$$\text{SN}_i = -10 \log \frac{1}{n} \left(\sum y_i^2 \right) \tag{11}$$

$$\text{SN}_i = -10 \log \frac{1}{n} \left(\sum \frac{1}{y_i^2} \right) \tag{12}$$

$\bar{y}_i$ is the mean value of the observations, $s_{y_i}^2$ is the variance of y, n is the number of observations and y is the observed data.

The objective of the experiment is to minimize the burr-height of PCB drilling, thus the smaller the better characteristics of the S/N ratio formula is used for analysis. Table 9 shows the mean and S/N ratios for each level.

Table 9
Experiment results for S/N ratio.

Experiment no.	Trial 1	Trial 2	Trial 3	Mean	SN ratio
1	60	59.2	64.2	61.13	−35.73
2	63	67	60	63.33	−36.04
3	34	37	34	35	−30.84
4	55	60	70	61.67	−35.84
5	19.6	20	25	21.53	−26.71
6	134.3	126.5	130	130.26	−42.29
7	50.4	48.4	48.4	49.06	−33.81
8	71	60	65	65.33	−36.32
9	70.1	72.5	60.7	67.76	−36.64

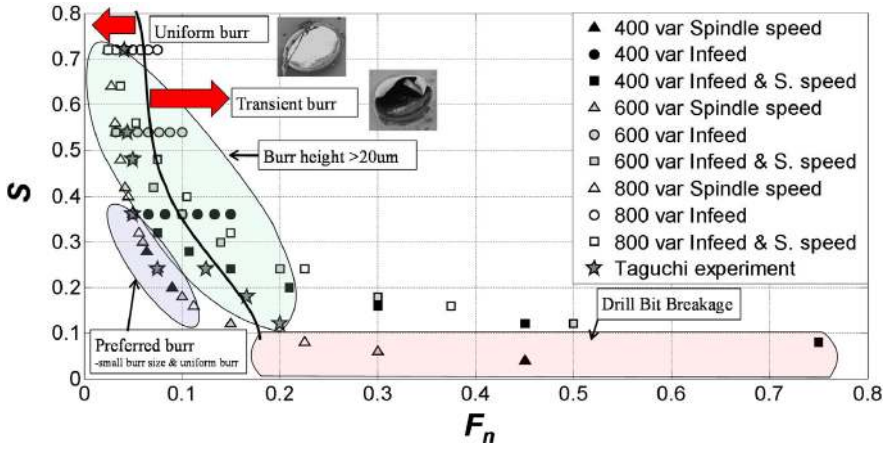

Fig. 11. M-DBCC chart showing burr types under various drilling conditions.

Table 10
Response table with the ranking of parameters influencing the drill burr height.

Level	Infeed	Spindle speed	Drill dia
1	−34.22	−36.61	−38.11
2	−34.95	−33.02	−36.17
3	−35.59	−35.13	−30.47
Δ = Max − Min	1.37	3.58	7.64
Ranking	3	2	1

In addition, response of each parameter on the burr-height was studied. The response of each parameter is shown in Table 10. The response table is created by calculating an average SN value for each factor using Eq. (13). From Table 10, it can be seen that drill diameter has the largest effect on the burr height.

$$SN_{parameter,level} = \frac{\sum SN}{NoL} \quad (13)$$

ΣSN is the sum of SN values corresponding to the parameter and level considered in the Taguchi orthogonal array. *NoL* is the number of levels. For example, $SN_{diameter,1} = (SN_1 + SN_6 + SN_8)/3$ or $SN_{infeed,3} = (SN_7 + SN_8 + SN_9)/3$.

7. Micro-drilling burr-control chart

Numerous parameters affect burr formation during drilling operations, as Table 1 indicates. The workpiece material is selected according to product requirements, while the tool material and geometry are usually standardized. The cutting speed and infeed are significant parameters, and are included in most drilling research. Based on our experimental results and burr classifications, a new M-DBCC was developed for micro-drilling on CCL double-sided PCBs. A complete burr chart can be used to predict the type of burr produced by various values of the drill diameter, infeed, and spindle speed for a given type of workpiece material. Fig. 11 shows the newly developed M-DBCC chart.

For each experiment performed, the parameters F_n and S were plotted as the abscissa and ordinate, respectively, of the burr chart. In accordance with the classification of burr shape, burr height, and tool breakage, the regions in the burr chart are classified into uniform burr, transient burr, preferred burr, drill breakage, and critical burr-height regions. The thick line denotes the boundary between uniform and transient burr types.

The Matlab function *convhull* was used to plot the critical burr-height region. Critical burr height is defined as a burr height greater than 20 μm, irrespective of burr type. The drill-bit breakage region was easily distinguished, since neither burr classification nor burr height measurement was needed. However, the boundary between uniform and transient burrs was not clearly distinguishable, and good judgment was required to distinguish between uniform and transient burrs that were close to the boundary. As described above, smaller drill bits produced larger burrs, while larger drill bits produced smaller burrs under the same drilling conditions. The preferred burrs (i.e., uniform burrs with minimal heights) are indicated in the diagram by the dark oval region.

8. Conclusions

DOE was used to develop a micro-drilling burr-control chart for a double-sided PCB with a laminated fiber-reinforced plastic (FRP) substrate. The classification of burrs and burr formation mechanisms into uniform and transient types was explained. The uniform burr region, transient burr region, preferred burr region, drill-bit breakage region, and critical burr-height region were plotted in the M-DBCC according to various classifications of PCB drilling burrs. The term 'critical burr height' was defined to indicate the region of greater burr height, irrespective of burr type. This M-DBCC can be used to predict and control burrs for a large range of cutting parameters.

Acknowledgements

This work was supported by the Brain Korea 21 project at Seoul National University, and the KITECH project funded by the Ministry of Knowledge Economy (No. 2010-TD-700203-001)

References

[1] Bhandari B, Hong Y-S, Yoon H-S, Lee J-C, Moon J-S, Dornfeld DA, et al. Development of micro drilling burr control chart based on Taguchi methods for PCB drilling. In: Asian Symposium for Precision Engineering and Nanotechnology 2011. 2011.
[2] Nakao Y, Watanabe Y. Measurement and evaluations of drilling burr profile. Proceedings of the Institution of Mechanical Engineers, Part B: Journal of Engineering Manufacture 2006;220:513–23.
[3] Chang P-C, Hsieh J-C, Wang C-Y. Adaptive multi-objective genetic algorithms for scheduling of drilling operation in printed circuit board industry. Applied Soft Computing 2007;7:800–6.
[4] Wang X, Wang LJ, Tao JP. Investigation of thrust in vibration drilling of fiber-reinforced plastics. Journal of Materials Processing Technology 2004;148:239–44.
[5] Takeyama H, Kato S. Burrless drilling by means of ultrasonic vibration. Annals of the CIPR 1991;41:83–6.
[6] Ko S-L, Chang J-E, Yang G-E. Burr minimizing scheme in drilling. Journal of Materials Processing Technology 2003;140:237–42.
[7] Chung I-Y, Kim J-D, Kang K-H. Ablation drilling of invar alloy using ultrashort pulsed laser. International Journal of Precision Engineering and Manufacturing 2009;10:11–6.

[8] Kim J, Min S, Dornfeld DA. Optimization and control of drilling burr formation of AISI 304L and AISI 4118 based on drilling burr control charts. International Journal of Machine Tools & Manufacture 2001;41:923–36.
[9] Gillespie LK. Burrs Produced by Drilling. Bendix Corporation Unclassified Topical Report; 1975.
[10] Watanabe H, Tsuzaka H, Masuda M. Microdrilling for printed circuit boards (PCBs) – influence of radial run-out of microdrills on hole quality. Precision Engineering 2008;32:329–35.
[11] Hinds BK, Treanor GM. Analysis of stresses in micro-drills using the finite element method. International Journal of Machine Tools & Manufacture 2000;40:1443–56.
[12] Dornfeld D, Lee D. Precision Manufacturing. New York: Springer; 2008.
[13] Aurich JC, Dornfeld D, Aeeazola PJ, Franke V, Leitz L, Min S. Burrs-analysis, control and removal. CIRP Annals-Manufacturing Technology 2009;58:519–42.
[14] Kang H-J, Ahn S-H. Fabrication and characterization of microparts by mechanical micromachining: precision and cost estimation. Proceedings of the Institution of Mechanical Engineers, Part B: Journal of Engineering Manufacture 2007;221:231–40.